HHS Public Access

Author manuscript

Ultrasound Med Biol. Author manuscript; available in PMC 2020 April 01.

Published in final edited form as:

Ultrasound Med Biol. 2019 April ; 45(4): 1010–1018. doi:10.1016/j.ultrasmedbio.2018.10.028.

Non-invasive small vessel imaging of human thyroid using motion-corrected spatiotemporal clutter filtering

Rohit Nayak[a,*], **Viksit Kumar**[b], **Jeremy Webb**[a], **Mostafa Fatemi**[b], and **Azra Alizad**[a]

[a]Department of Radiology, Mayo Clinic College of Medicine and Science, Rochester, Minnesota, 55902, United States

[b]Department of Physiology and Biomedical Engineering, Mayo Clinic College of Medicine and Science, Rochester, Minnesota, 55902, United States

Abstract

Reliable assessment of small vessel blood flow in thyroid, without using any contrast agents, can be challenging due to increased physiological motion as a consequence of its proximity to the pulsating carotid artery. In this study, we hypothesized that correction of tissue motion prior to singular value decomposition (SVD) based clutter filtering, can improve the coherency of the tissue components, and thus allow better clutter suppression and visualization of small vessels in the thyroid.

We corroborated this hypothesis by conducting phantom and *in vivo* studies using a clinical ultrasound scanner, implemented with compounded plane wave imaging. The phantom studies were conducted using a homogeneous tissue-mimicking phantom, to study the impact of motion on the covariance of the spatiotemporal data, in the absence of blood activity. The non-invasive *in vivo* study was conducted on a 74 yr old female with a suspicious thyroid nodule. A rigid body based motion correction was performed using tissue displacements obtained from 2D normalized cross-correlation based speckle tracking. Subsequently, the power Doppler images were computed using SVD based spatiotemporal clutter filtering.

The results from the phantom study demonstrated that motion can considerably reduce the covariance of the spatiotemporal data, and thus increase the rank of the tissue components. Upon subjecting the phantom to a total translation displacement of 6 pixels over the entire ensemble, in each direction (axial and lateral), the covariance dropped by over 25%. The results obtained from the non-invasive *in vivo* study demonstrated that visualization of small vessel blood flow improved with motion correction of the power Doppler ensemble. The contrast-to-noise ratio of the blood signal in motion corrected power Doppler image was considerably higher (8.17 and 8.32 dB), compared to that obtained using the standard SVD approach at optimal (0.87 and 4.33 dB) and a lower singular value threshold (1.92 and 3.05 dB). Further, the covariance of the *in vivo* thyroid spatiotemporal data increased by approximately 10% with motion correction.

[*]Corresponding Author: Azra Alizad (alizad.azra@mayo.edu).

These preliminary results show the ability of using motion correction to improve the visualization of small vessel blood flow in thyroid, without using any contrast agents. The results of this feasibility study were encouraging, and warrant further development and more *in vivo* validation in moving tissues and organs.

Keywords

Power Doppler; Motion Correction; Cross-correlation; Microvasculature; Small Vessel Imaging; Thyroid; Compounded Plane Wave Imaging

Introduction

Clutter suppression is a crucial step in visualizing blood flow with pulse wave power Doppler (PD). In conventional PD studies, clutter is primarily suppressed by high-pass filtering of the slow-time ensemble. This is performed under the assumption that tissue motion is primarily of low velocity and thus corresponds to low frequency, compared to blood flow which is relatively of higher velocity (Alfred and Lovstakken, 2010). However,in the presence of large physiological and sonographer's hand motion, tissue frequencies can be similar or even higher than that of slow blood flow (Tierney et al., 2017). This can limit the visualization of small vessel blood flow, which can be of low frequency (or velocity) because of small vessel diameter (Thomas and Sumam, 2016). In a recent study,Tierney et. al. (Tierney et al., 2017) proposed an adaptive demodulation based techniqueto minimize any spectral broadening of the tissue components due to motion, for improved clutter suppression.

Demene *et. al.* demonstrated that non-invasive visualization of small vessel blood flow can be substantially improved by utilizing the spatiotemporal characteristic of the Doppler ensemble (Demené et al., 2015). Specifically, ultrafast acquisition enables tissue components to acquire low rank in the Casorati matrix due to its higher temporal and spatial coherence compared to the incoherent flow of blood, and thus a singular value rank based thresholdingcould be effectively used for clutter rejection. However, in the presence of large and cyclic physiological motion and sonographer hand motion, the spatiotemporal coherence of the Doppler ensemble can degrade, thus leading to sub-optimal clutter filtering. A specific example of accidental motion in *in vivo* human neonate brain imaging was discussed in (Demené et al., 2015). Motion increased the rank of the tissue components, and therefore a higher singular value (SV) threshold was used to suppress tissue clutter. However, the scope of increasing SV threshold without consequently eliminating any small vessels in the PD image may be limited. Specifically for thyroid, which is typically associated with large pulsating motion due to its proximity to the carotid artery, non-invasive imaging of flow in small vessels can be challenging. Visualization of small vessel blood flow can be improved by injecting micro-bubble based contrast agents in the blood stream. However, its associated with increased complexity, cost and invasiveness.

Normalized cross-correlation (NCC) based speckle tracking has been the gold standard for high quality motion estimation in ultrasound imaging (Viola and Walker, 2003), and has been widely used for blood flow imaging, (Trahey et al., 1987), elastographic imaging

(Ophir et al., 2002; Greenleaf et al., 2003; Parker et al., 2010), temperature imaging (Varghese et al., 2002), phase-aberration correction (Ng et al., 1994). In this paper, we used a 2D NCC based speckle tracking technique to estimate tissue displacements, which were subsequently used for motion correction. The hypothesis of this paper is that correction of tissue motion prior to SVD based filtering can improve the coherency of the tissue components, and thus allow better clutter suppression and improved visualization of small vessels. This is based on recently reported studies that used a similar approach for motion correction (Hingot et al.,2017; Foiret et al., 2017), for ultrasound contrast agent based micro-vasculature imaging using micro-bubbles. The efficacy of their technique was demonstrated on a rat model,and the results showed an improvement in the definition of the renal micro-vessels, which were otherwise blurred due to motion. In non-contrast agent based blood flow imaging, the signal from blood flow in small vessels can be up to 60–80 dB lower than that of tissue.However, motion correction of the Doppler ensemble can be potentially useful in increasing the signal power of the small vessel blood flow (Hingot et al., 2017), and thus enhance its visualization. The goal of this study was to assess the feasibility of using motion corrected Doppler ensemble for non-invasive *in vivo* small vessel imaging of human thyroid. We tested the hypothesis by conducting *in vivo* imaging of the thyroid gland using a clinical ultrasound scanner implemented with compounded plane wave imaging.

The following sections describe the methods used in phantom and *in vivo* studies.

Methods

Data Acquisition

The ultrasound IQ data for the phantom and *in vivo* experiments were acquired using an Alpinion E-Cube 12R ultrasound scanner (Alpinion Medical Systems Co., Seoul, South Korea), equipped with a L12–3H linear array probe. The scanner transmitted and received using 128 and 64 elements, respectively. The plane wave (PW) IQ data was acquired using 7 compounding angles, with a maximum angle of 3° and an incremental step-size of 1° (Montaldo et al., 2009; Nayak et al., 2017b; Denarie et al., 2013), at a transmit frequency of 11.5 MHz. Specifically, each B-mode image was computed by transmitting 7 angular plane waves (−3°, −2°, −1°, 0°, 1°, 2°, 3°) and the corresponding received signals were compounded to form a single image. This process was repeated sequentially to acquire 1848 compounded images in 3 seconds for imaging depth of 35 mm. The imaging pulse repetition frequency (PRF) was 8624 Hz. However, the final imaging frame rate reduced to 616 Hz, due to (1) seven angle plane wave compounding, and (2) the scanner needed two receive events (with 64 elements in each) to create a single image. Accordingly, the frame rate was 8624 Hz/7/2 = 616 Hz. The received RF signal was sampled at 40 MHz. The beam-formed images obtained from the E-Cube 12R had dimensions of 960 × 192 pixels in depth and width, respectively.The axial and lateral length of each pixels were 38.5 μm and 200 μm, respectively. The speed of sound was assumed to be 1540 m/s for the calculation of beam-forming delays.

Phantom Study

The goal of the phantom study was to evaluate the impact of tissue motion on the spatiotemporal covariance and the singular value decay of the Doppler ensemble, in a controlled environment. The experiments were conducted using a homogeneous tissue-mimicking custom LE series phantom from Gammex (Middleton, WI, USA) that had an attenuation coefficient slope of 0.5 dB/cm/MHz (McFarlin et al., 2015). The scatterers (Potters 3000E Speriglass) had a concentration of 5.7g/l, and a diameter range of 5–40 micrometers. The phantom data was acquired using the data acquisition setup described in the previous section.To acquire data without any motion, the linear array probe was clamped to a rigid stand. Using this data, nine different instances of rigid body translational motion were realized in MATLAB (Mathworks, MA, US) by shifting the rows (axially) and columns (laterally) of Doppler frames by a total of 3, 6 and 18 pixels for the entire ensemble of 1848 frames.Specifically, the phantom images were shifted to produce a total displacement of 3, 6 and 18 pixels, in the uniaxial, unilateral and diagonal directions. The sub-pixel displacements between consecutive frames were achieved by using a spline based sub-pixel interpolation (Parker et al., 1983; Konofagou and Ophir, 1998; Huntzicker et al., 2014). Motion was introduced in post-processing specifically to prevent any potential out-of plane motion or speckle decorrelation. Therefore, in the absence of any blood activity, out of plane motion or speckle decorrelation, any loss in covariance of the spatiotemporal data could be specifically attributed to in-plane translational motion. Further, the phantom data was acquired with the same parameters as used in *in vivo* thyroid study.

In vivo Study

The *in vivo* study was conducted to evaluate the feasibility of using motion corrected ultrasound data to improve the visualization of small vessel flow in the thyroid, using a clinical ultrasound scanner. The ultrasound data was obtained from a 74 years female with a suspicious thyroid nodule, which was recommended for US-guided fine-needle aspiration biopsy. The study was approved by the Mayo Clinic institutional review board, and a written consent was obtained from the patient prior to their participation. The ultrasound data was acquired by an experienced sonographer, across the longitudinal cross-section of the right thyroid gland, prior to the biopsy of the nodule. Further, the subject was asked to hold her breath for the 3s duration of the scan to minimize any motion due to breathing.

Displacement Estimation and Motion Correction

The axial and lateral displacements associated with the *in vivo* ultrasound data were estimated using a 2D cross-correlation based echo tracking algorithm. The ultrasound images were tracked using a 2D kernel (0.2 mm × 0.8 mm), which overlapped by 90% in both coordinates. A 2D spline interpolator was used to compute sub-pixel displacement estimates. Further, the images were interpolated in the axial and lateral direction by a factor of 3 and 10, respectively (Parker et al., 1983; Konofagou and Ophir, 1998; Huntzicker et al., 2014). The images were interpolated to increase the spatial density of the correlation functions. This is specifically important for estimating lateral motion, since ultrasound has no phase information in the direction perpendicular to beam propagation (Konofagou and Ophir,1998). The 2D cross-correlation based displacement tracking was performed on a

GTX 1080 Ti GPU (Nvidia Corp., CA, US). The processing time for tracking two ultrasound frames using a Xeon 2.3 GHz (Intel, CA, US) CPU processor with 36 cores was 68.47 ± 0.21 seconds.Comparatively, the processing time using the NVidia GTX 1080 Ti GPU, with 10 teraflops single precision power was 2.8 ± 0.03 seconds. Overall, we achieved an approximate 24.5 times gain in processing time using the GPU over the CPU for this application.

The estimated axial and lateral displacements maps were transformed from Eulerianto Lagrangian co-ordinates, to correspond with the first frame of the Doppler ensemble. Subsequently, motion correction of the Doppler ensemble was performed to re-register each ultrasound frame with that of the first frame, by globally shifting the rows and columns by the cumulated estimated displacements. Specifically, the mean axial and lateral displacements obtained from each frame, averaged over the demarcated tumor region, were used to correct for motion. Further, the real and imaginary components of the IQ data were tracked and motion corrected independently, prior to the power Doppler estimation.

Power Doppler Imaging

The original and the motion corrected ultrasound data was clutter filtered using the singular value decomposition of the spatiotemporal Casaroti matrix (Demené et al., 2015)

$$S_{blood} = S(x, z, t) - \sum_{r=1}^{r=th} U_r \lambda_r V_r^* \quad 1$$

where the matrices S and S_{blood} represent pre- and post-clutter filtered Doppler ensemble.The matrices U, V consist of left and right singular orthonormal vectors, respectively. The corresponding singular values and their order are denoted by λ_r and r, respectively, and $*$ represents conjugate transpose. Based on the decay of the SV order, a global threshold (th) of 420 was empirically chosen to separate tissue clutter from blood signal. Subsequently, the power Doppler signal was computed using the following equation:

$$PD(x, z) = \sum_{t=1}^{N_t} \left| S_{blood}(x, z, t) \right|^2 \quad 2$$

where N_t denotes the ensemble length. The background separation in the PD image was achieved by using a top-hat morphological filter, with a disc-shaped structuring element of radius 5 pixels (Bayat et al., 2017).

Data Analysis

The contrast to noise ratio (CNR) of the PD images was computed as follows :

$$CNR = \frac{E\left[S_{vessel}\right]}{E\left[S_{background}\right]} \quad 3$$

where, $E[.]$ is the mean operator, and S_{vessel} and $S_{background}$ denote blood vessel and background signal in the PD image, respectively. Further, the covariance of the spatiotemporal data was computed using normalized zero mean complex signals of the Casorati matrix.

Results

Phantom study

Figure 1 displays the SV decay and co-variance associated with the spatiotemporal data of a homogeneous tissue-mimicking phantom. Motion was induced (a) uniaxially, (b) unilaterally and (c) in both axial and lateral directions. (a-c) shows that in the absence of motion, tissue signals were predominantly low rank, and the singular values decayed rapidly with increase in rank order. When the phantom was subjected to motion, there was a noticeable increase in the rank of the spatiotemporal matrix. Specifically, the decay of the singular values changed from steep to gradual with increase in tissue motion. Figures (d-o) displays the covariance of the spatiotemporal matrix. The covariance was highest (~1) in the absence of motion (d,h,l), but gradually decreased with increase in motion (e-g, i-k,m-o). For example, in the absence of motion, average spatial covariance was 0.99 ± 0.00012, however, when motion of 3, 6 and 18 pixels was induced diagonally (l-o), it gradually reduced to 0.865 ± 0.104, 0.73 ± 0.19, 0.6071 ± 0.263 and 0.393 ± 0.31, respectively. Further, the loss of covariance due to axial motion was observed to be higher than lateral motion. This was primarily because axial has high frequency phase information compared to lateral that can rapidly decorrelate, for the same amount of pixel motion. This was also observed in the SV decay plots (a,b). Especially for the example with motion of 18 pixels, the singular values in range of 1–10, which specifically represented tissue signal, the decay was relatively steeper for lateral motion compared to that in the axial direction.

Patient Study

Figure 2 displays the *in vivo* sonogram and PD images of the thyroid gland obtained using SVD based clutter filtering. (a) displays the compounded plane wave sonogram. The PD images obtained with and without motion correction is displayed in (c) and (b), respectively, clutter filtered using the same optimal SV threshold (420). (d) displays the PD image corresponding to the Doppler ensemble used in (b), however at a lower SV threshold (220) to increase the contribution from small vessels without any motion correction. Further, the PD insets for the five ROIs highlighted in the sonogram(b) were displayed in (e-g), (h-j),(k-m), (o-q), and (r-t), and they corresponded to blue, magenta, green, cyan and yellow ROIs, respectively. The outline of thyroid nodule is indicated in white in the sonogram. The results show that the motion corrected PD image (c) noticeably improved the visualization of the small vessels compared to that obtained without any motion correction (b,d). These results are consistent with previously reported studies conducted using micro-bubble based contrast agents which used a similar motion correction technique to improve visualization of micro-

vessels in rats (Hingot et al., 2017; Foiret et al., 2017). Further, the CNR of the blood vessel (green ROI) indicated in (l), corresponding to (b-d) were 0.87 dB, 8.17 dB and 1.92 dB, respectively. Similarly, for another instance indicated in (p), the CNR of the blood vessels corresponding to (b-d) were 4.33, 8.32 and 3.05 dB, respectively. The CNR values were computed by considering the region outlined in blue as the signal and the rest of the rectangular region in the green ROI (l,p) as background. The diameter of the thyroid vessels in insets (o-p), were estimated to be between 200 – 800 microns.

Figure 3 displays the mean axial (a,c) and lateral (b,d) displacements associated with the thyroid gland. (a,b) displays the axial and the lateral displacements obtained from each consecutive frame, respectively. (c, d) displays the corresponding accumulated axial (a) and lateral (b) displacements, respectively. The displacements reported in (a-d) were averaged over the entire thyroid gland that was identified and outlined by an expert sonographer.The axial and lateral displacements estimated using the 2D normalized cross-correlation were observed to be very similar to those reported in carotid artery elastography studies (Kawasaki et al., 2009; Larsson et al., 2015). This was primarily due to the anatomical position of the carotid artery, which is located laterally with respect to the thyroid gland.Further, an steady amount of translation motion can also be observed, primarily in the lateral direction, possibly due to the slipping of the nodule during the image acquisition.

Figure 4 displays (a) the SV decay and (c,d) the spatiotemporal covariance associated with the *in vivo* thyroid images. The results show that the motion corrected ultrasound images had a more rapid decay and a higher spatiotemporal covariance than otherwise. The covariance of the spatiotemporal matrix increased from 0.73 ± 0.13 to 0.83 ± 0.09. These observations were consistent with the results obtained from the phantom study. Figure (b) displays the motion vector associated with the thyroid nodule, cumulated over the entire Doppler ensemble.

Discussion

In this paper, we investigated the feasibility of using motion corrected ultrasound data for improved visualization of small vessel blood flow in thyroid, and compared it performance with the global SVD approach (Demené et al., 2015).

A low rank matrix is typically identified to have redundant columns, which in the Casorati form is analogous to high temporal coherence of the spatial points (Demené et al., 2015). However, in the presence of motion, increased variability across the Casorati columns (temporal dimension) can lead to an increase in the rank and a corresponding decrease in covariance of the Casorati matrix. The experimental results obtained from a homogeneous tissue-mimicking phantom demonstrated that motion can considerably reduce the covariance of the the spatiotemporal matrix. Specifically, for a simulated motion of 6 pixels in axial and lateral direction, the mean covariance of the spatiotemporal matrix decreased by over 25 % (Fig. 1(b)). The rank of the spatiotemporal data was predominantly low in the absence of motion and blood activity. However, it increased noticeably with increase in motion (Fig. 1(a)). Further, the decorrelation of the spatiotemporal data due to axial motion was observed to be higher than lateral motion in the singular value decay plots (**a,b**) and the covariance

maps (**d-k**). Correspondingly, the decay of first ten singular values in the (**c**),which represents motion in combined axial and lateral direction, was observed to be similarto that obtained from uniaxial motion (**a**) than (**b**), thus indicating that the decorrelationof the spatiotemporal data due to axial motion was relatively higher than that in the lateral direction. This was primarily because axial has high frequency phase information compared to lateral that can rapidly decorrelate, for the same amount of pixel motion.

Figure 2 demonstrates the in vivo efficacy of the proposed technique using a clinical ultrasound scanner, for small vessel imaging of thyroid. The PD image computed using motion corrected ultrasound data (c) demonstrated a noticeable improvement in visualization of small vessels, relative to those obtained using conventional SVD based clutter filtering (b, d). Some of the low contrast vessels that were not visible in the standard SVD based PD image (b), were partially recovered by lowering the SV threshold (d), however, at the cost of increase in tissue clutter and background noise. This can be more clearly visualized in representative insets displayed in (e-t). For example, in (h-j), (o-q), and (r-t), a branch of the small vessel was poorly visible in the conventional SVD images for both thresholds (h, j, o, q, r, t), however, its visualization could be noticeably improved by motion correction (i, p, s). The CNR of the blood vessel indicated in the inset (l, p) increased by 7.3 dB (8.2 – 0.9) and 4.0 (8.3 – 4.3) with motion correction, respectively, relative to that obtained using the regular SVD approach. Further, consistent with the observations of the phantom study, covariance and rank of the spatiotemporal matrix of the in vivo thyroid data improved with motion correction (Fig. 4). The mean covariance of the spatiotemporal data increased by 10% with motion correction. These preliminary results highlight the advantage of using motion corrected Doppler ensemble for in vivo thyroid small vessel imaging. Additionally, the utility of the proposed technique is not limited to the SVD based approach of Doppler imaging, and could be potentially useful in reducing overall tissue motion in classical approach to clutter filtering (Foiret et al., 2017).

The primary significance of using ultrafast acquisition for non-contrast Doppler imaging is that it can minimize the overall tissue motion associated with acquiring large Dopplerensembles. This allows conserving the high spatiotemporal coherence of tissue components,which is important for effective discrimination between tissue and blood signal (Demené et al., 2015). However, ultrafast imaging is a resource intensive feature, which is limitedprimarily to high-end clinical scanners. The technique proposed in this paper can be helpful in improving the performance of SVD based Doppler imaging in mid-range clinical scanners,which may have relatively lower frame-rate due to reduced number of receive channels.Lower frame-rates can increase the impact of motion. Specifically, the *in vivo* efficacy of the proposed technique was demonstrated using a clinical ultrasound scanner, which acquired data with only on 64 of 128 transducer channels at a time, thereby reducing the imaging frame-rate by half. Further, reductions in frame-rate could also be due to need for angular compounding of plane wave acquisitions, which enables significant improvements in image quality (Montaldo et al., 2009; Nayak et al., 2017b; Korukonda et al., 2013). Accordingly,loss of covariance due to motion from low frame-rate can potentially be minimized by using motion correction, as proposed in this manuscript. Another important scope of motion correction for Doppler flow imaging, which is currently our work in

progress, is to achieve ultra-long coherent image acquisition, which can substantially boost the performance of Doppler imaging of blood flow in small and micro vessels.

Estimation of lateral displacements using ultrasound can be challenging due to lack of phase information in the direction orthogonal to the beam propagation. However, several researchers have demonstrated the efficacy of using compounded plane wave imaging to address this issue, and have used it for non-invasive carotid elastography (Nayak et al., 2017b; Korukonda et al., 2013; Nayak et al., 2017a; Hansen et al., 2010, 2016; Nayak et al., 2018). The cross-correlation coefficient associated with tracking of subsequent frames were consistently over 0.95. However, the cross-correlation coefficient obtained from tracking of individual frames wi th reference to the first frame decreased rapidly, to 0.49 ± 0.2 and 0.299 ± 0.23 over the first 25% and 50 % of the frames in the Doppler ensemble, respectively.This was primarily due to the gradual out of plane motion of the thyroid nodule, which was also evident in the B-mode image sequence. However, since high frame rate of acquisition was used, the out of plane motion for subsequent frames were negligible. This was one of the primary reasons for using a rigid body based motion correction technique, to re-register Doppler frames while preserving their local spatial distribution.

In our future work, we will address this limitation by using a localized, adaptive SVD based approach, similar to that reported in (Song et al., 2017). This will allow motioncorrection in smaller local blocks that can be reasonably assumed to have uniform displacements. This approach will also enable reduction of tissue clutter observed in the near-field sub-cutaneous layers, which are typically hard to suppress using a global SVD approach.The age of the female subject used for *in vivo* imaging was not representative of thyroid cancer cases, which is a limitation of the patient recruitment protocol of this preliminary study. In future studies, a broad, representative group of patients will be considered for small vessel imaging of thyroid. We also plan to fabricate and use small vessel imaging phantoms (Grand-Perret et al., 2018) for assessing the efficacy of the proposed technique in a controlled environment, and also to study the impact of motion on image registration that can lead to incoherency in Doppler integration (Hingot et al., 2017).

Conclusion

In this study, we demonstrated that motion corrected Doppler ensemble could improve the performance of SVD-based clutter filtering for *in vivo* visualization of small vessels in the thyroid gland, without using contrast agents. Previously used approach of changing the SV threshold to overcome the impact of motion could only partially recover the blood signal, however, at the cost of increased tissue clutter. The preliminary results obtained using the proposed approach demonstrated that motion correction improved the covariance of the spatiotemporal matrix and reduced the rank of the tissue components, resulting in improved clutter filtering and visualization of small vessels in thyroid.

Acknowledgments

This study was supported by National Institutes of Health (NIH) grants R01CA148994,R01CA168575, R01CA195527, R01CA174723, and R01EB17213. The content is solely the responsibility of the authors and does

not necessarily represent the offcial views of NIH.We would also like to thank Nvidia Corp. for donating the GPU that was used for motion tracking in this study.

References

Alfred C, Lovstakken L. Eigen-based clutter filter design for ultrasound color flow imaging: a review. IEEE transactions on ultrasonics, ferroelectrics, and frequency control, 2010;57.

Bayat M, Fatemi M, Alizad A. Background-free visualization of microvasculature networks. In: Ultrasonics Symposium (IUS), 2017 IEEE International IEEE, 2017 pp. 1–1.

Demené C, Deffieux T, Pernot M, Osmanski BF, Biran V, Gennisson JL, Sieu LA, Bergel A, Franqui S, Correas JM, et al. Spatiotemporal clutter filtering of ultrafast ultrasound data highly increases doppler and fultrasound sensitivity. IEEE transactions on medical imaging, 2015;34:2271–2285. [PubMed: 25955583]

Denarie B, Tangen TA, Ekroll IK, Rolim N, Torp H, Bjåstad T, Lovstakken L. Coherent plane wave compounding for very high frame rate ultrasonography of rapidly moving targets. IEEE Trans Med Imaging, 2013;32:1265–76. [PubMed: 23549887]

Foiret J, Zhang H, Ilovitsh T, Mahakian L, Tam S, Ferrara KW. Ultrasound localization microscopy to image and assess microvasculature in a rat kidney. Scientific reports,2017;7:13662. [PubMed: 29057881]

Grand-Perret V, Jacquet JR, Leguerney I, Benatsou B, Grégoire JM, Willoquet G, Bouakaz A, Lassau N, Pitre-Champagnat S. A novel microflow phantom dedicated to ultrasoud microvascular measurements. Ultrasonic Imaging, 2018:0161734618783975.

Greenleaf JF, Fatemi M, Insana M. Selected methods for imaging elastic properties of bio-logical tissues. Annual review of biomedical engineering, 2003;5:57–78.

Hansen HH, de Borst GJ, Bots ML, Moll FL, Pasterkamp G, de Korte CL. Validation of non-invasive *in vivo* compound ultrasound strain imaging using histologic plaque vulnerability features. Stroke, 2016;47:2770–2775. [PubMed: 27686104]

Hansen HH, Lopata RG, Idzenga T, de Korte CL. An angular compounding technique using displacement projection for noninvasive ultrasound strain imaging of vessel cross-sections. Ultrasound in medicine & biology, 2010;36:1947–1956. [PubMed: 20850217]

Hingot V, Errico C, Tanter M, Couture O. Subwavelength motion-correction for ultrafast ultrasound localization microscopy. Ultrasonics, 2017;77:17–21. [PubMed: 28167316]

Huntzicker S, Nayak R, Doyley MM. Quantitative sparse array vascular elastography: The impact of tissue attenuation and modulus contrast on performance. Journal Of Medical Imaging, 2014;1:027001–027001. [PubMed: 26158040]

Kawasaki T, Fukuda S, Shimada K, Maeda K, Yoshida K, Sunada H, Inanami H, Tanaka H, Jissho S, Taguchi H, et al. Direct measurement of wall stiffness for carotid arteries by ultrasound strain imaging. Journal of the American Society of Echocardiography, 2009;22:1389–1395. [PubMed: 19880276]

Konofagou E, Ophir J. A new elastographic method for estimation and imaging of lateral displacements, lateral strains, corrected axial strains and poisson's ratios in tissues. Ultra-sound in Medicine and Biology, 1998;24:1183–1199.

Korukonda S, Nayak R, Carson N, Schifitto G, Dogra V, Doyley MM. Noninvasive vascular elastography using plane-wave and sparse-array imaging. Ultrasonics, Ferroelectrics and Frequency Control, IEEE Transactions on, 2013;60:332–342.

Larsson M, Heyde B, Kremer F, Brodin LÅ, D'hooge J. Ultrasound speckle tracking for radial, longitudinal and circumferential strain estimation of the carotid artery–an in vitro validation via sonomicrometry using clinical and high-frequency ultrasound. Ultrasonics, 2015;56:399–408. [PubMed: 25262347]

McFarlin BL, Kumar V, Bigelow TA, Simpson DG, White-Traut RC, Abramowicz JS,O'Brien WD. Beyond cervical length: A pilot study of ultrasonic attenuation for early detection of preterm birth risk. Ultrasound in Medicine and Biology, 2015;41:3023–3029. [PubMed: 26259887]

Montaldo G, Tanter M, Bercoff J, Benech N, Fink M. Coherent plane-wave compounding for very high frame rate ultrasonography and transient elastography. IEEE Trans. On Ultrasonics, Ferroelectrics and Frequency Control, 2009;56:489–506.

Nayak R, Huntzicker S, Ohayon J, Carson N, Dogra V, Schifitto G, Doyley MM. Principal strain vascular elastography: Simulation and preliminary clinical evaluation. Ultrasound in Medicine & Biology, 2017a.

Nayak R, Schifitto G, Doyley MM. Noninvasive carotid artery elastography using multi-element synthetic aperture imaging: Phantom and *in vivo* evaluation. Medical physics, 2017b;44:4068–4082. [PubMed: 28494102]

Nayak R, Schifitto G, Doyley MM. Visualizing angle-independent principal strains in the longitudinal view of the carotid artery: Phantom and *in vivo* evaluation. Ultrasound in Medicine and Biology, 2018;44:1379–1391. [PubMed: 29685590]

Ng GC, Worrell SS, Freiburger PD, Trahey GE. A comparative evaluation of several algo-rithms for phase aberration correction. IEEE transactions on ultrasonics, ferroelectrics,and frequency control, 1994;41:631–643.

Ophir J, Alam SK, Garra BS, Kallel F, Konofagou EE, Krouskop T, Merritt CR, Righetti R, Souchon R, Srinivasan S, et al. Elastography: imaging the elastic properties of soft tissues with ultrasound. Journal of medical ultrasonics, 2002;29:155. [PubMed: 27277961]

Parker JA, Kenyon RV, Troxel DE. Comparison of interpolating methods for image resampling. IEEE Transactions on medical imaging, 1983;2:31–39. [PubMed: 18234586]

Parker KJ, Doyley MM, Rubens DJ. Imaging the elastic properties of tissue: the 20 year perspective. Physics in medicine & biology, 2010;56:R1. [PubMed: 21119234]

Song P, Manduca A, Trzasko JD, Chen S. Ultrasound small vessel imaging with block-wise adaptive local clutter filtering. IEEE transactions on medical imaging, 2017;36:251–262. [PubMed: 27608455]

Thomas B, Sumam K. Blood flow in human arterial system-a review. Procedia Technology, 2016;24:339–346.

Tierney J, Coolbaugh C, Towse T, Byram B. Adaptive clutter demodulation for non-contrast ultrasound perfusion imaging. IEEE transactions on medical imaging, 2017;36:1979–1991. [PubMed: 28622670]

Trahey GE, Allison JW, Von Ramm OT. Angle independent ultrasonic detection of blood flow. IEEE Transactions on Biomedical Engineering, 1987:965–967. [PubMed: 2961682]

Varghese T, Zagzebski J, Lee F. Elastographic imaging of thermal lesions in the liver *in vivo* following radiofrequency ablation: preliminary results. Ultrasound in Medicine and Biology, 2002;28:1467–1473. [PubMed: 12498942]

Viola F, Walker WF. A comparison of the performance of time-delay estimators in medical ultrasound. IEEE transactions on ultrasonics, ferroelectrics, and frequency control, 2003;50:392–401.

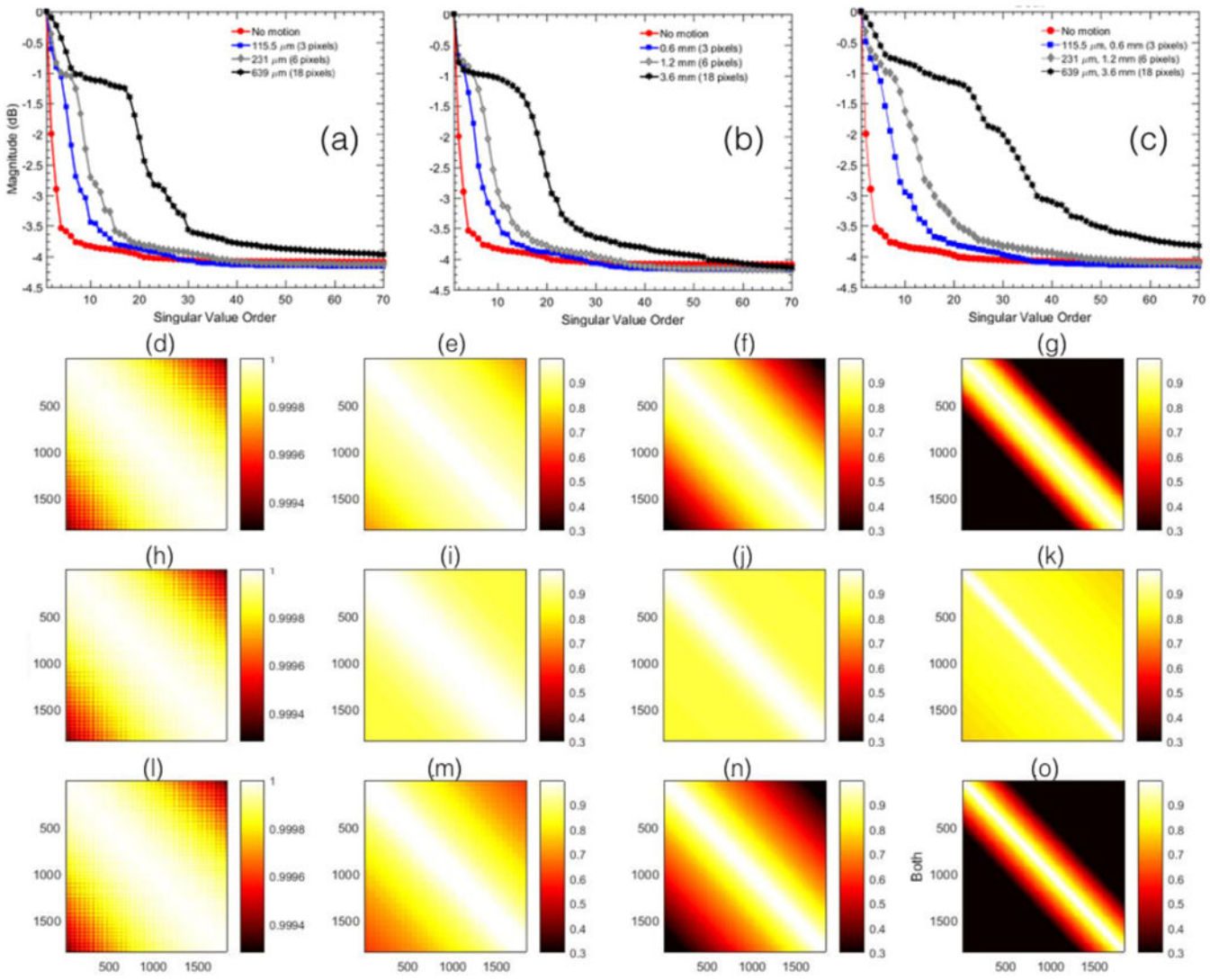

Figure 1.

displays the singular value order and covariance of the spatiotemporal Casaroti matrix obtained from the homogeneous phantom data with no blood activity. (a-c) displays the variation in the decay of the singular value order of the phantom data, with respect to increasing extent of motion in uniaxial, unilateral and diagonal directions, respectively. The corresponding covariance of the spatiotemporal Casaroti matrix obtained in the absence of motion is displayed in (d,h,l), and in the presence of motion3 (e,i,m), 6 (f,j,n) and 18 (g,k,o) pixels. Rows (e-g), (i-k), and (m-o) represents uniaxial, unilateral and diagonal motion, respectively.

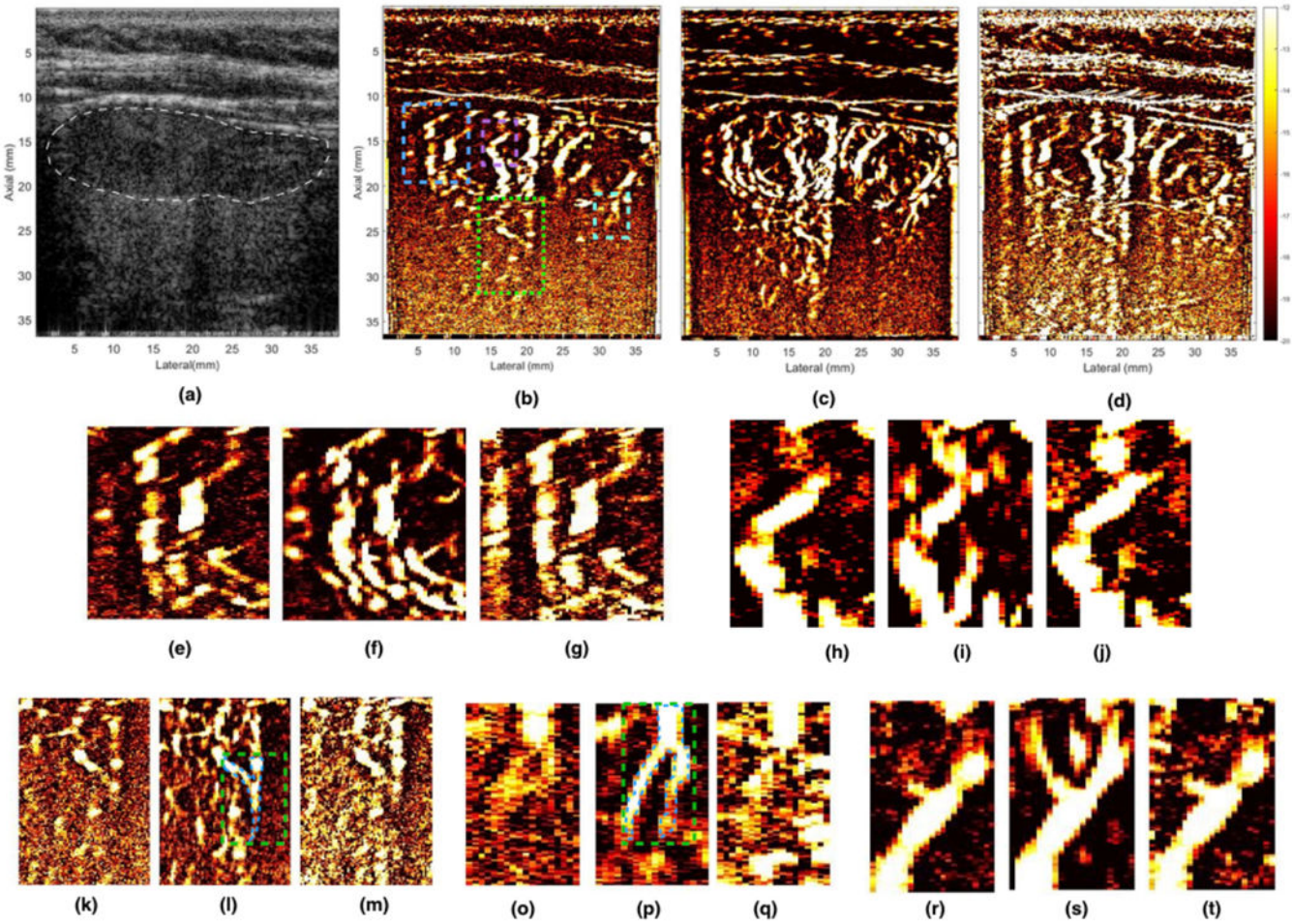

Figure 2.

displays the representative in vivo B-mode and PD image of the thyroid nodule, obtained using SVD based clutter filtering. (a) displays the PW sonogram, (b, c) displays the PD image, pre- and post-motion correction, respectively, thresholded at the same SV threshold (420). (d) displays PD image corresponding to (b), but at a lower SV threshold (220), to allow increased contribution from blood signal, which may have been suppressed with clutter in (b). Figures (e, h, k, o, r) show zoomed insets obtained from (b). Figures (f, i, l, p, s) show zoomed insets obtained from (c). Figures (g, j, m, q, t) show zoomed insets obtained from (d). The ROI for the five zoomed insets have been outlined in the (b), where blue, magenta, yellow, green and cyan regions corresponds to (e-g), (h-j), (k-m), (o-q), and (r-t), respectively. The location of the nodule has been indicated in white in the sonogram (a). The CNR metric was calculated from the vessels indicated in green ROIs (l, p).

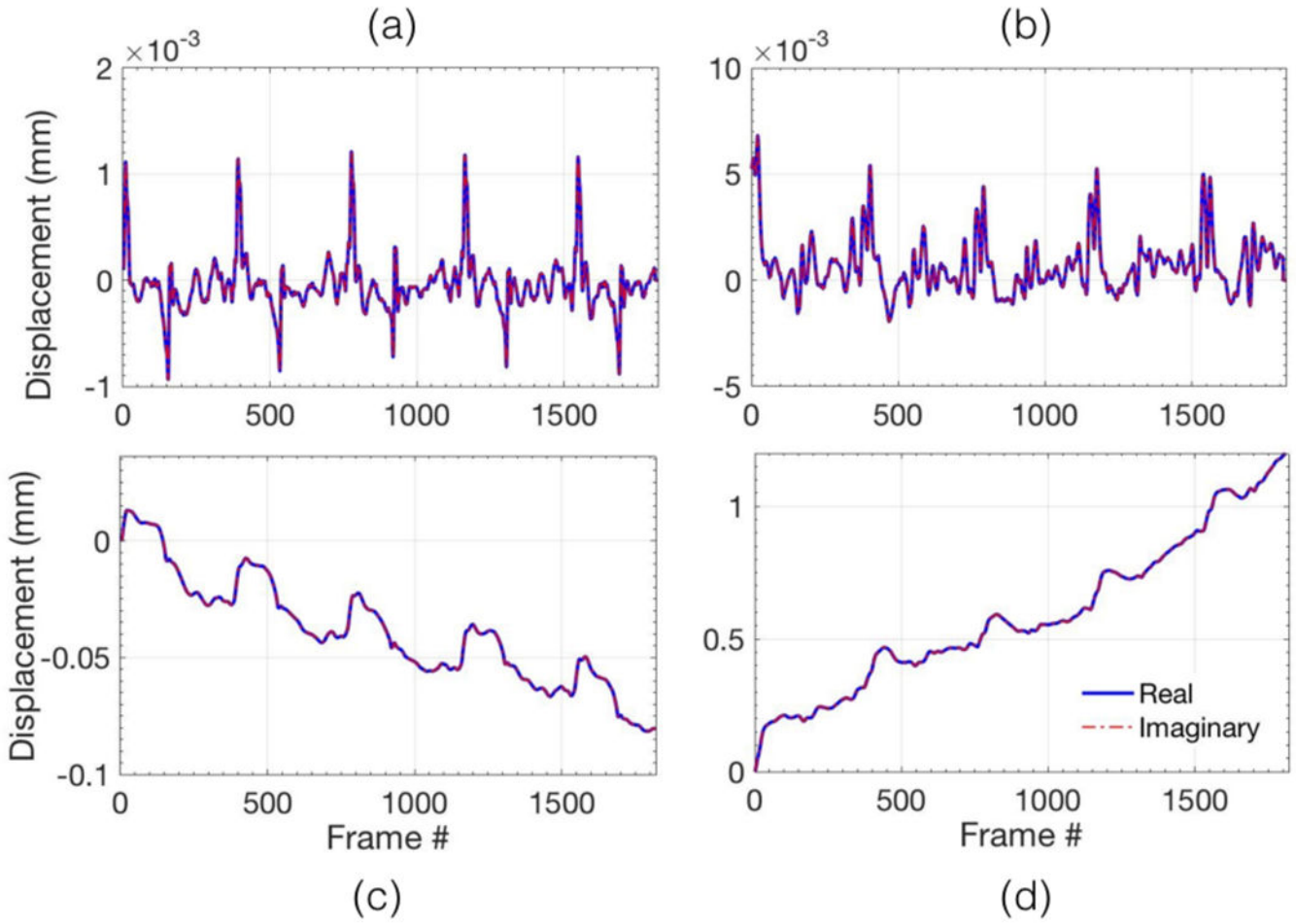

Figure 3.

(a,c) and (b,d) visualize the axial and lateral displacements respectively for acquisition of 3 second of ultrafast compounded plane wave data. The top row displays the displacements associated with every consecutive frame, and the bottom row displays the total accumulated displacements, with reference to the first frame in the ensemble.

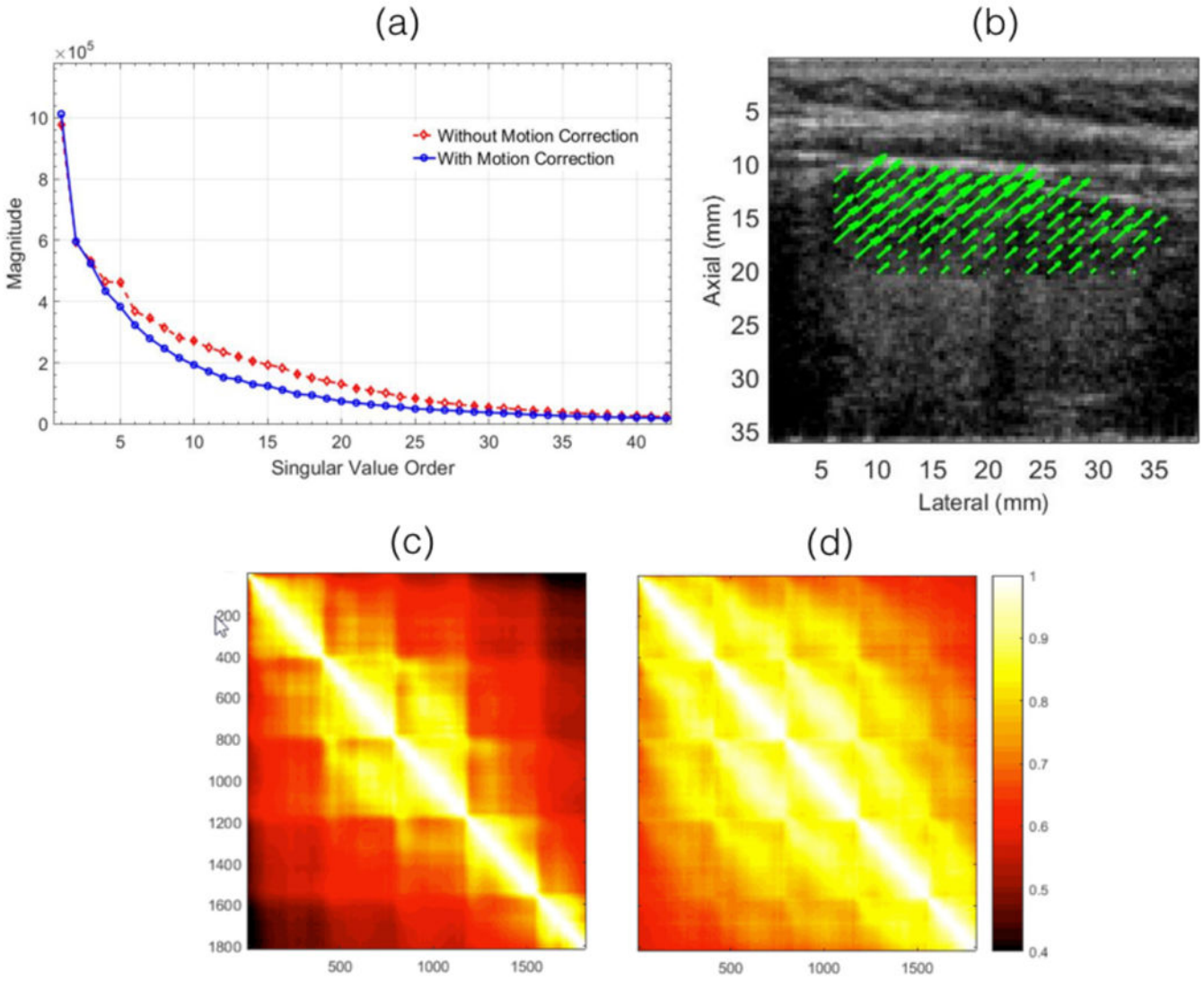

Figure 4.

displays the the singular value order and covariance of the spatiotemporal Casaroti matrix associated with the in vivo thyroid images. (a) displays the singular value decay associated with pre- and post-motion corrected data. The covariance of the pre- and post-motion corrected spatiotemporal matrix is displayed in (c) and (d), respectively. (b) displays the 2D motion vectors associated with the thyroid nodule.